

000	glu2011coarsegreen28	glu2011coarseglu2011coarsegreen28	054
001			055
002	secondauthor@i2.org		056
003			057
004			058
005			059
006			060
007			061
008			062
009			063
010			064
011			065
012			066
013			067
014			068
015			069
016			070
017			071
018			072
019			073
020			074
021			075
022			076
023			077
024			078
025			079
026			080
027			081
028			082
029			083
030			084
031			085
032			086
033			087
034			088
035			089
036			090
037			091
038			092
039			093
040			094
041			095
042			096
043			097
044			098
045			099
046			100
047			101
048			102
049			103
050			104
051			105
052			106
053			107

108
109
110162
163
164111 **Partial Matching of 3D Shapes using Deformable Diversity**112
113
114165
166
167115
116
117168
169
170118
119
120171
172
173121
122
123174
175
176**Abstract**124
125
126
127
128
129
130
131
132177
178
179
180
181
182
183
184
185
186
187
188
189
190
191
192
193
194
195
196
197
198
199
200
201
202
203
204
205
206
207
208
209
210
211
212
213
214
215

We propose a novel approach for the matching of partial deformable shapes in 3D. Inspired by recent advances in 2D template matching techniques, our method relies on the concept of deformable diversity similarity(DDIS), extends and adapts it from an image to the 3D shape domain, and leverages the distinct behavior of this framework in different scales to achieve shape correspondences. We evaluate this framework on the SHREC16 partial matching of deformable shapes and show state of the art performance in achieving sparse correspondences.

133
134
135**1. Introduction**136
137
138
139
140
141
142
143
144
145
146
147
148
149
150
151
152
153
154
155188
189
190
191
192
193
194
195
196
197
198
199
200
201
202
203
204
205
206
207
208
209
210
211
212
213
214
215

Shape correspondence is a fundamental and challenging problem in computer vision and graphics. It has usage in various applications such as transferring texture and animation. Shapes rarely, if ever manifest in only one pose. While rigid transformations between surfaces is a well researched topic with many adequate solutions, a more challenging problem arises when a shape is deformed non-rigidly, a case all too common for people, animals and objects. Moreover, the shape acquisition process almost always lead to partiality of the scanned object. Occlusions arise from different angles of acquisition, which cause an object to occlude itself, or stem from other occluding objects. An additional type of difficulty which might be occur is topological noise, occurring when shapes touch pn another, thus making sensors unable to seperate them. All of these combined give rise to the challenging problem of partial correspondences, where a deformed and incomplete shape, possibly with topological changes, has to be matched with its full version. The goal of this paper is to deal with this challenging problem.

156
157
158
159
160
161206
207
208
209
210
211
212
213
214
215

While in a rigid setting the problem can be solved by RANSAC and ICP like approaches[23, 10], extending these to non-rigid case produces mediocre results due to an underlying assumption of small deformations. Early methods specialized for the non-rigid problem focused on minimization of intrinsic metric distortion[6, 32] and regularity of

parts[?, 4]. These methods all contain with them a global assumption of isometry which holds only approximately, these tended to break down with it, and are also unable to handle extreme partiality. Another family of method is based on functional correspondence. These methods model correspondences as a linear operator of a known nature between a space of functions on manifolds[17]. These methods, originally designed for the full shape correspondence scenario have achieved state of the art results on various partial matching tasks in the recent years[14, 33, 21], and produce dense correspondence maps, but are not parallelizable, and their reliance on intrinsic metrics makes them invariant to symmetry.

We take a different approach. We take advantage of the fact that while the isometric property tends to break over large distances, it usually holds approximately in limited environments. These also tend to suffer a lot less from boundary effects, especially when concentrated around the extremities of a shape.

We can thus treat the problem of partial correspondences as matching of multiple templates, each smaller then the partial surface centered around shape landmarks.

In addition, since point descriptors are known to be modified by partiality and deformations, instead of using them directly, we follow the approach off[30](DDIS) which tackles template matching in 2D and use simple statistical assumptions on the nature of nearest neighbors between small patch descriptors, along with the assumption of an approximate conservation of distances in medium environments to obtain similarity scores between these partial shape templates.

We analyze the behavior of DDIS similarity in different scales and devise a multi scale scheme which leverages the advantages of each scale while masking their shortcomings.

We show that using this approach, we are able to generate a set of sparse correspondences, which are less prone to symmetrical assignment than functional correspondence reliant methods, and are of superior quality on the SHREC16 Partial matching challenge[8]. We then demonstrate how these sparse correspondences can be used as an input to existing functional correspondence algorithms to obtain dense

Anonymous CVPR submission

Paper ID ****

216 correspondences or a higher quality. In summary, our
217 contributions are:
218

- 219 • A non trivial extension of Deformable Diversity from
220 2 to 3 Dimensions.
- 221 • A modified DDIS similarity measure which is more
222 well suited to handle matching of templates with a differ-
223 ent number of points.
- 224 • An empirical analysis of DDIS behavior in different
225 scales, leading to an improved multi-scale framework.
- 226 • A novel multi-template approach to partial matching
227 of deformable shapes which can both produce state of
228 the art sparse correspondences, and be used as an input
229 to functional correspondence algorithms, significantly
230 improving the results obtained by these.

231 The rest of the work is organized as follows: in section
232 2 we go over related works in the field of shape analysis.
233 Section 3 introduces our Deformable Diversity framework
234 for 3D shape matching. Experiments and results are given
235 in section 4, and the conclusions are in section 5.

236 2. Related work

237 2.1. Matching Of Deformable Surfaces

238 As a fundamental problem in computer graphics and vi-
239 sion, an extensive body of work have been done on the
240 matching of surfaces. A variety of shape descriptors have
241 been devised for this task which can be roughly divided in
242 to 2 families. Extrinsic ones, such as PFH[24], SHOT[31]
243 and FPFH[23] which are usually calculated in euclidean
244 space and are thus sensitive to non rigid deformations, but
245 can discern between reflections and are also more robust to
246 noise, topological artifacts and boundary effects. On the
247 other hand intrinsic features such as Heat[7] and Wave Ker-
248 nel signatures[2] are invariant under isometric transfor-
249 mations, but are very sensitive to partiality and are unable to
250 discern between symmetric parts. These have been com-
251 monly used to generate rough correspondences between
252 surfaces and point clouds based on their similarity, but are
253 noisy and offer little in terms of bijectivity and continu-
254 ity of the solution. a measure of global consistency us-
255 ing these can be achieved by solving an energy minimization
256 problem of the disimilarity matrices stemming from an assign-
257 ment, and the auction algorithm has been commonly em-
258 ployed for this purpose. Other methods use pairwise re-
259 lations between points such as geodesic distances[26, 27,
260 $\check{g}lu2011coarse$ – $\check{g}lu2011coarse$], and search for a configura-
261 tion which minimizes the distortions of these. These meth-
262 ods usually carry a high complexity, both due to calculating
263 the pairwise relations, and the combinatorial configuration
264 search, and are thus either obtain sparse matches[26, 27,

265 $\check{g}lu2011coarse$ – $\check{g}lu2011coarse$] to alleviate this complexity,
266 or used strategies such as coarse to fine solutions. Another
267 common approach has been to embed the shapes into a dif-
268 ferent lower dimension “canonical” space, this has been
269 done by generalized MDS[6], an embedding into the mo-
270 bius group[13], or by representation in the LBO basis[29].
271 A notable family of works are derived from functional cor-
272 respondences. Introduced at[17, 19, 12, 33] these assume
273 that functions can be mapped from one manifold to an-
274 other via a linear operator, finding this transfer operator
275 allows to embed point in a space where the ICP method
276 can obtain correspondences. Lately there has been a large
277 body of works which employ learning methods such as Ran-
278 dom Forests[20] and deep learning architectures[15, 3, 16].
279 These show the promise of achieving state of the art per-
280 formance, but require a lot of annotated data.

281 2.2. Partial Matching of Deformable shapes

282 The introduction of partiality adds complications which
283 are not present in the full correspondence scenario. Spectral
284 quantities change drastically, while geodesic paths dis-
285 appear. For the rigid setup, the Iterative Closest Point(ICP)[1]
286 algorithm, preceded by initial alignment[25] tackle partial
287 matching successfully. Adapting this to the rigid setup how-
288 ever has proved to have limited success due to the alignment
289 which is necessary, and thus is only fit for very small non-
290 rigid deformation.

291 Early works which were designed with partial match-
292 ing in mind[4, 5] formulated an energy minimization prob-
293 lem over metric distortion and regularity of correspond-
294 ing parts. Following works relaxed the regularity require-
295 ment by allowing for sparse correspondences[32, 22]. Other
296 works[27, 26] minimized the distortion metric over the
297 shape extremities by doing combinatorial search of least
298 distortion matches and then densify them while employing
299 a refining scheme in the process.

300 In[18] a bag of words point-wise descriptors on a part in
301 conjunction with a constraint on area similarity and the reg-
302 ularity of the boundary length to produce correspondence
303 less matching parts without point to point correspondences
304 by energy minimization.

305 Another line of works employ machine learning tech-
306 niques to learn correspondences between manifolds. Re-
307 cently [21] had proven that partiality induces a slanted di-
308 agonal structure in the correspondence matrix and found
309 the Laplacian eigenfunctions from each basis which induces
310 this structure. Current state of the art[14] uses this notion in
311 conjunction with joint diagonalization. The main drawback
312 of this method, shared with other intrinsic methods, is its
313 invariance to symmetries.

314 3D Shape Descriptors

324
325
326
327
328
329
330
331
332

2.3. Template matching in 2D

Template matching in 2D is a well researched topic. Similarly to 3D objects are going complex deformations of pose, and are only seen partially depending on the camera point of view. Recently a series of works which use a very simplistic framework based on the statistical properties of nearest neighbors in low level feature space had made good strides in tackling this complex task.

Best Buddies Similarity Great strides had been achieved in the field of 2D template matching. Best Buddies Similarity[9] is a simple framework which employs a statistical assumption - if two regions \mathcal{N}, \mathcal{M} contain the same template patches should maintain Bi Directional Similarity. That is - given a point $n_i \in \mathcal{N}$ and a corresponding point $m_i \in \mathcal{M}$ they should point to each other as nearest neighbors - that is if $NN_{\mathcal{M}}(n_i) = m_j$ then on a matching template we should expect $NN_{\mathcal{N}}(m_j) = n_i$. Solving for a matching template then amounts to finding the region which has the highest count of best buddies. This amazingly simple scheme has been shown to be able to handle occlusions, missing parts and complex deformations of templates.

Deformable Diversity Similarity Building upon the above work, [30] relaxed the requirement for a best buddy relation, and added a requirement for spatial coherency.

The rather cumbersome best buddy relation has been relaxed to requiring only that the diversity of the set of nearest neighbors sets between corresponding templates should be high. This is actually prerequisite to a high best buddies similarity score and serves as a rough approximation of it. For this end diversity is formally defined as:

$$DIS = c \cdot |\{n_i \in \mathcal{N} : \exists m_j \in \mathcal{M}, NN(m_j, \mathcal{N}) = n_i\}| \quad (1)$$

where $|\cdot|$ denotes group size and $c = 1/\min(|\mathcal{M}|, |\mathcal{N}|)$ is a normalization factor. Between non corresponding windows, indeed one should expect most points to have no real corresponding point, and thus be mapped to a very and remote nearest neighbors. On the other hand, regions containing matching objects are drawn from the same distribution, thus the diversity of nearest neighbors should be high. To accommodate this assumption not only did they reward high diversity of nearest neighbors, but also penalized mapping to the same patch. To this end, another, a negative diversity measure had been defined:

$$\kappa_{\mathcal{M}}(n_i) = |\{m \in \mathcal{M} : NN^a(m, \mathcal{N}) = n_i\}| \quad (2)$$

With x_i^a denoting the appearance descriptor of point x_i . Thus the contribution of a patch $m_j : NN^a(m_j, \mathcal{N}) = n_i$ is $\exp(1 - \kappa_{\mathcal{M}}(n_i))$. An additional observation made has been that while non isometric deformations do occur, they should be restricted, small, in real objects. With distance on the window pixel grid between 2 nearest neighbor points

defined as $r_j = d(m_j^l, n_i^l)$ with x_i^l denoting the location of x_i on a grid, the final Deformable Diversity Similarity formulation becomes:

$$DDIS = c \sum_{\mathcal{N} \rightarrow \mathcal{M}} \frac{1}{1 + r_j} \cdot \exp(1 - \kappa(NN^a(m_j, \mathcal{N}))) \quad (3)$$

3. General Approach

Given two surfaces \mathcal{M} and \mathcal{N} , the goal is to find the best match of \mathcal{N} within \mathcal{M} . Our approach is based on AT: XXXX key ideas, which we describe hereafter.

AT: Nadav, this paragraph (key ideas) is a mess. A key idea is NOT how you implemented it (e.g. DDIS), but rather what lies behind it. Re-write it. One key to our method is the assumption that while non rigid deformations and partiality leads to changes in the data, the underlying shape distributions from which the shapes on the surfaces are drawn should remain highly overlapping, and thus the data points drawn from these should be spread approximately uniformly, one inside the other, leading to a high diversity of nearest neighbors. However, since unlike in[30] we don't have the benefit of having a template and a query of the same size in the absence of a grid, and the space of geometric shapes is more constrained than that of RGBXY, one should not expect a near bijection.

Another assumption is that of a geometrical coherency - geodesic distances of corresponding pairs of points on a shape and a roughly isometrically deformed version of which should hold approximately leading us to use the assumption of low distortion. However, the preservation of distances holds only approximately even for full template matching, and even less so in the presence of partiality and topological noise. It holds that the longer a distance between 2 points is, the more likely it is that a distortion had occurred on the geodesic path between them, either due to a non isometric deformation, partiality removing a piece of the geodesic path or topological noise introducing a shortcut. It follows from this that the smaller the pieces we are trying to match will be, the higher the likelihood of pairwise distances to be preserved should be.

Therefore, our algorithm, which is illustrated in Figure XXX, consists of the following steps.

1. Pre-processing.

- Dense shape descriptor fields are calculated for both shapes.
- Approximate nearest neighbor field is used in the shape descriptor space to obtain the Nearest Neighbor Field.

2. Sampling.

- Shape extremities are extracted as an initial set of samples.

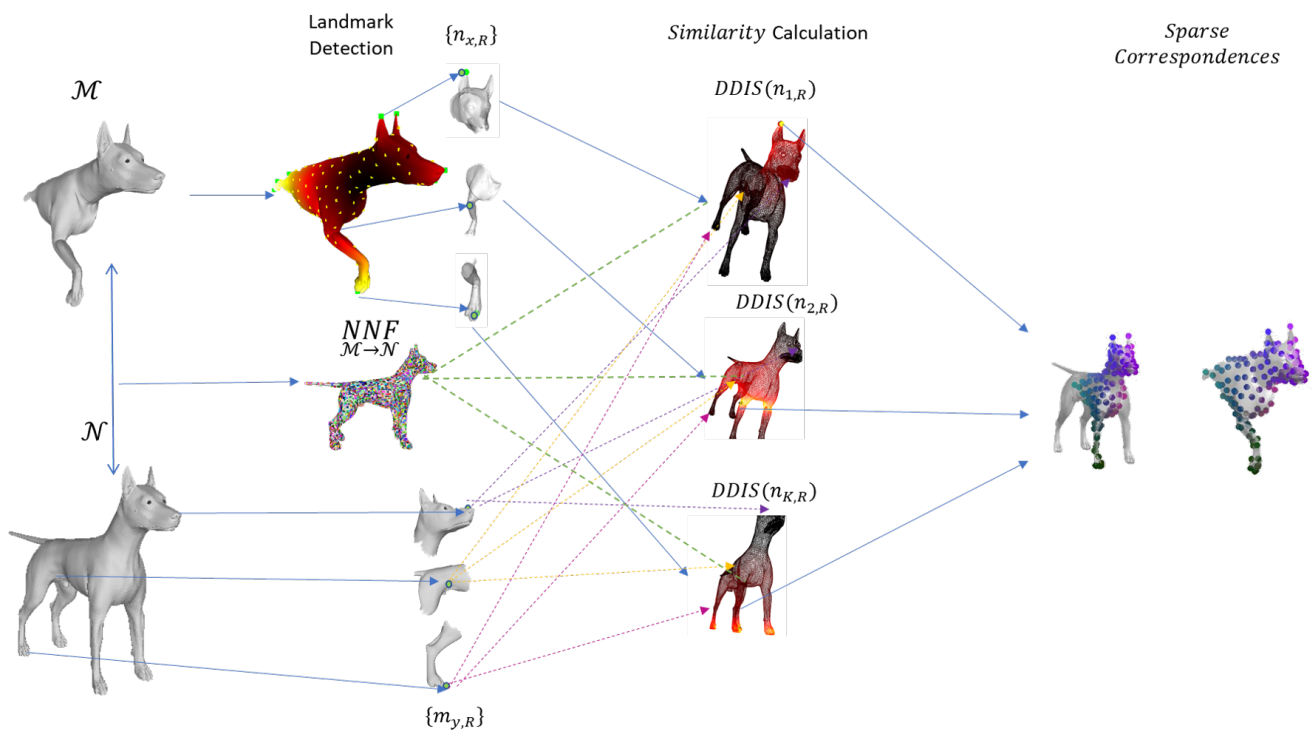


Figure 1. High level illustration of the DDIS Partial Correspondence pipe.

- The set is iteratively expanded to obtain a set covering the entire part.

3. Similarity Calculation- to obtain a set of correspondences we calculate similarity score between the samples and every point

- For each sample point geodesic discs of radii R_T is defined as its template.
- Deformable Diversity score is calculated between the geodesic discs surrounding each point on the model and the sample point templates.
- Correspondences are then determined for each sample point by taking the point in the model which achieve the maximal similarity score w.r.t. to it.

Refinement. The goal of this stage is to achieve better correspondences based on simple global tests and constraints

- 4.
- Correspondences which exhibit high distortion are determined are marked as not trusted.
 - For Correspondences which are deemed not trusted we search among the local maximas of the DDIS score a point which minimizes their distortion w.r.t to trusted point.

3. Outline of the algorithm (Preprocessing (normal estimation, FPFH), Finding the landmark points, computing DDIS correspondence for pairs, computing correspondence of surfaces) Include an image of this general overview.

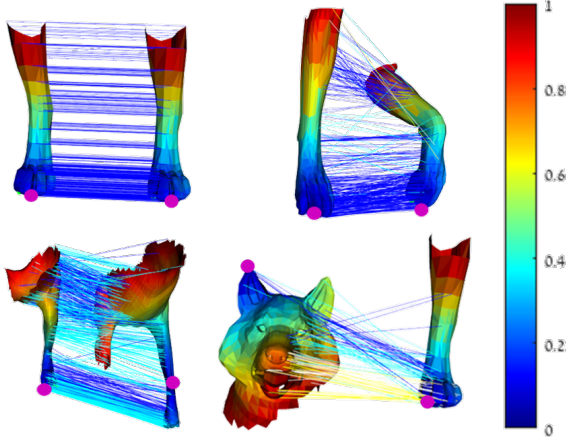
3.1. Algorithm Outline

The following pipeline is employed to obtain a sparse set of point-wise correspondences. We first calculate dense point-wise descriptor field by obtaining mesh normals and calculating FPFH shape descriptors for every points on both meshes. Then the FPFH space nearest neighbor of every point in \mathcal{M} in \mathcal{N} is calculated - this is denoted the nearest neighbor field. The surface \mathcal{N} is sampled quasi uniformly by iteratively choosing a sample, marking all the vertices in a radius around it and setting the unmarked vertex with minimal distance to the marked set as our next sample, obtaining a set of samples S which covers \mathcal{N} . A template s_{i,R_T} around each point $s_i \in S$ is then obtained by extracting a geodesic disc of a radius R_T around it. We then traverse every point $m_j \in \mathcal{M}$, and calculate the deformable diversity similarity score between its surrounding geodesic disc m_{j,R_T} to each sample template. We determine our initial sparse correspondence set $\S = \{(s_i, \hat{m}_i)\}$ by setting for each p the points \hat{m}_i whose geodesic disc \hat{m}_{i,R_T} similarity s_{i,R_T} is maximal. We then filter out matches which have a high distortion score and use a greedy search for a better match for these from the set of local similarity maximas.

432
433
434
435
436
437
438
439
440
441
442
443
444
445
446
447
448
449
450
451
452
453
454
455
456
457
458
459
460
461
462
463
464
465
466
467
468
469
470
471
472
473
474
475
476
477
478
479
480
481
482
483
484
485
486
487
488
489
490
491
492
493
494
495
496
497
498
499
500
501
502
503
504
505
506
507
508
509
510
511
512
513
514
515
516
517
518
519
520
521
522
523
524
525
526
527
528
529
530
531
532
533
534
535
536
537
538
539

540 4. Road-map to the section We will begin with a de-
 541 scription of the changes made for the deformable diversity
 542 framework as a result of moving from 2D to 3D. We will
 543 then go over the specific stages of preprocessing necessary
 544 for Deformable Diversity in 3D. We will continue with de-
 545 scribing the matching process of a single mini template on
 546 a full shape. Finally we will describe the extraction of mul-
 547 tiple correspondences using this framework.
 548

549 550 **4. Deformable Diversity Similarity in 3D**
 551



555 556 557 558 559 560 561 562 563 564 565 566 567 568
 569 570 571 572 573 574 575 576 577
 578 579 580 581 582 583 584 585 586 587 588 589 590 591 592 593
 Figure 2. Illustration of Diversity Similarity between different shapes. Geodesic Distances are color coded by the jet scheme. You can notice that on identical pieces, and even on deformed matching pieces there are multiple diverse matches, most of which are colored in blue to indicated very similar distances from the source point, whereas on different pieces most lines map to very few points and a lot of yellow lines (high deformation) exist

578 The nature of 3D data gives rise to unique problems
 579 which do not occur in the 2D scenario. Data is distributed in
 580 space both sparsely and with varying densities - the amount
 581 of data points occupying a given volume can vary drasti-
 582 cally. A second problem arises from the absence of a reg-
 583 ular grid. These problems require different definitions for
 584 key components to the 2D deformable diversity formula-
 585 tion. For this work we chose the image patch to be replaced
 586 by a neighborhood which is required to calculate a selected
 587 shape descriptor, usually a small sphere in euclidean space
 588 or a surface patch with a radius r_F . The search window of
 589 a template is defined as a geodesic disc around the query
 590 point, with a radius denoted by R_T . The pixel grid distance
 591 is replaced by either a euclidean distance $d_{Euc}(x^l, y^l)$ (in the
 592 case of point clouds) or geodesic distance $d_{Geo}(x^l, y^l)$ (for
 593 surface meshes). Given these DDIS between shape parts

594 595 \mathcal{M}_{x,R_T} and \mathcal{N}_{y,R_T} can be naively formulated as:
 596 597 598

$$DDIS = c \cdot \sum_{m_j \in \mathcal{M}_{x,R_T}} \frac{\exp(1 - \kappa(NN^S(m_j, \mathcal{N}_{y,R_T})))}{1 + r_j} \quad (4)$$

599 600 where \mathcal{M}_{x,R_T} and \mathcal{N}_{y,R_T} are the shape parts in a radius R_T
 601 602 603 surrounding the points $x \in \mathcal{M}$ and $y \in \mathcal{N}$ respectively, r_j
 604 605 606 is the induced deformation
 607 608

$$r_j = \frac{|d(m_j^l, m_x^l) - d(NN^S(m_j, \mathcal{N}_{y,R_T})^l, n_y^l)|}{\gamma \cdot R_T} \quad (5)$$

609 610 , where γ is a selected fraction and c is a normalization co-
 611 612 613 efficient $c = 1/\min|\mathcal{N}_{y,R_T}|, |\mathcal{M}_{x,R_T}|$.
 614 615 616

617 618 However, we wouldn't like to penalize our similarity
 619 620 621 score in case of repeating patterns or symmetrical shapes
 622 623 624 which have both symmetries in the template search win-
 625 626 627 dow. Intuitively and empirically the exponent is too harsh
 626 627 628 and indeed unnecessary as both deformity and diversity will
 627 628 629 attenuate the score in case of multiple nearest neighbors. On
 628 629 630 the other hand, we wouldn't want to reward far correspon-
 629 630 631 dences at all because they are unlikely to originate from a
 630 631 632 corresponding patch.
 631 632

632 633 To account for this the following formulation has been
 633 634 635 found to work better: given a point $n_i \in \mathcal{N}_{y,R_T}$ has a set
 634 635 636 of nearest neighbors in descriptor space on a geodesic disc
 635 636 637 $\mathcal{M}_{n_i} = \{m_j \in \mathcal{M}_{x,R_T} : NN^S(m_j, N_{y,R_T}) = n_i\}$, we
 636 637 638 define $m'_i = \operatorname{argmin}_{m_j \in \mathcal{M}_{n_i}}(r_j)$ and r'_i the minimal distortion dis-
 637 638 639 tance, we add only the contribution of this point to the sim-
 638 639 640 ilarity score which then becomes
 639 640 641

$$DDIS(N_{y,R_T}, \mathcal{M}_{x,R_T}, \gamma) = \sum_{m'_i} \frac{1}{1 + r'_i} \quad (6)$$

642 643 644
 643 644 645
 644 645 646
 645 646 647
 explain why – can we see it visually on the same exam-
 ple?added both qualitative(visual, and quantitative example

647 648 649
 648 649 650
 649 650 651
 650 651 652
 651 652 653
 652 653 654
 653 654 655
 654 655 656
 655 656 657
 656 657 658
 657 658 659
 658 659 660
 659 660 661
 660 661 662
 661 662 663
 662 663 664
 663 664 665
 664 665 666
 665 666 667
 666 667 668
 667 668 669
 668 669 670
 669 670 671
 670 671 672
 671 672 673
 672 673 674
 673 674 675
 674 675 676
 675 676 677
 676 677 678
 677 678 679
 678 679 680
 679 680 681
 680 681 682
 681 682 683
 682 683 684
 683 684 685
 684 685 686
 685 686 687
 686 687 688
 687 688 689
 688 689 690
 689 690 691
 690 691 692
 691 692 693
 692 693 694
 693 694 695
 694 695 696
 695 696 697
 696 697 698
 697 698 699
 698 699 700
 699 700 701
 700 701 702
 701 702 703
 702 703 704
 703 704 705
 704 705 706
 705 706 707
 706 707 708
 707 708 709
 708 709 710
 709 710 711
 710 711 712
 711 712 713
 712 713 714
 713 714 715
 714 715 716
 715 716 717
 716 717 718
 717 718 719
 718 719 720
 719 720 721
 720 721 722
 721 722 723
 722 723 724
 723 724 725
 724 725 726
 725 726 727
 726 727 728
 727 728 729
 728 729 730
 729 730 731
 730 731 732
 731 732 733
 732 733 734
 733 734 735
 734 735 736
 735 736 737
 736 737 738
 737 738 739
 738 739 740
 739 740 741
 740 741 742
 741 742 743
 742 743 744
 743 744 745
 744 745 746
 745 746 747
 746 747 748
 747 748 749
 748 749 750
 749 750 751
 750 751 752
 751 752 753
 752 753 754
 753 754 755
 754 755 756
 755 756 757
 756 757 758
 757 758 759
 758 759 760
 759 760 761
 760 761 762
 761 762 763
 762 763 764
 763 764 765
 764 765 766
 765 766 767
 766 767 768
 767 768 769
 768 769 770
 769 770 771
 770 771 772
 771 772 773
 772 773 774
 773 774 775
 774 775 776
 775 776 777
 776 777 778
 777 778 779
 778 779 780
 779 780 781
 780 781 782
 781 782 783
 782 783 784
 783 784 785
 784 785 786
 785 786 787
 786 787 788
 787 788 789
 788 789 790
 789 790 791
 790 791 792
 791 792 793
 792 793 794
 793 794 795
 794 795 796
 795 796 797
 796 797 798
 797 798 799
 798 799 800
 799 800 801
 800 801 802
 801 802 803
 802 803 804
 803 804 805
 804 805 806
 805 806 807
 806 807 808
 807 808 809
 808 809 810
 809 810 811
 810 811 812
 811 812 813
 812 813 814
 813 814 815
 814 815 816
 815 816 817
 816 817 818
 817 818 819
 818 819 820
 819 820 821
 820 821 822
 821 822 823
 822 823 824
 823 824 825
 824 825 826
 825 826 827
 826 827 828
 827 828 829
 828 829 830
 829 830 831
 830 831 832
 831 832 833
 832 833 834
 833 834 835
 834 835 836
 835 836 837
 836 837 838
 837 838 839
 838 839 840
 839 840 841
 840 841 842
 841 842 843
 842 843 844
 843 844 845
 844 845 846
 845 846 847
 846 847 848
 847 848 849
 848 849 850
 849 850 851
 850 851 852
 851 852 853
 852 853 854
 853 854 855
 854 855 856
 855 856 857
 856 857 858
 857 858 859
 858 859 860
 859 860 861
 860 861 862
 861 862 863
 862 863 864
 863 864 865
 864 865 866
 865 866 867
 866 867 868
 867 868 869
 868 869 870
 869 870 871
 870 871 872
 871 872 873
 872 873 874
 873 874 875
 874 875 876
 875 876 877
 876 877 878
 877 878 879
 878 879 880
 879 880 881
 880 881 882
 881 882 883
 882 883 884
 883 884 885
 884 885 886
 885 886 887
 886 887 888
 887 888 889
 888 889 890
 889 890 891
 890 891 892
 891 892 893
 892 893 894
 893 894 895
 894 895 896
 895 896 897
 896 897 898
 897 898 899
 898 899 900
 899 900 901
 900 901 902
 901 902 903
 902 903 904
 903 904 905
 904 905 906
 905 906 907
 906 907 908
 907 908 909
 908 909 910
 909 910 911
 910 911 912
 911 912 913
 912 913 914
 913 914 915
 914 915 916
 915 916 917
 916 917 918
 917 918 919
 918 919 920
 919 920 921
 920 921 922
 921 922 923
 922 923 924
 923 924 925
 924 925 926
 925 926 927
 926 927 928
 927 928 929
 928 929 930
 929 930 931
 930 931 932
 931 932 933
 932 933 934
 933 934 935
 934 935 936
 935 936 937
 936 937 938
 937 938 939
 938 939 940
 939 940 941
 940 941 942
 941 942 943
 942 943 944
 943 944 945
 944 945 946
 945 946 947
 946 947 948
 947 948 949
 948 949 950
 949 950 951
 950 951 952
 951 952 953
 952 953 954
 953 954 955
 954 955 956
 955 956 957
 956 957 958
 957 958 959
 958 959 960
 959 960 961
 960 961 962
 961 962 963
 962 963 964
 963 964 965
 964 965 966
 965 966 967
 966 967 968
 967 968 969
 968 969 970
 969 970 971
 970 971 972
 971 972 973
 972 973 974
 973 974 975
 974 975 976
 975 976 977
 976 977 978
 977 978 979
 978 979 980
 979 980 981
 980 981 982
 981 982 983
 982 983 984
 983 984 985
 984 985 986
 985 986 987
 986 987 988
 987 988 989
 988 989 990
 989 990 991
 990 991 992
 991 992 993
 992 993 994
 993 994 995
 994 995 996
 995 996 997
 996 997 998
 997 998 999
 998 999 1000
 999 1000 1001
 1000 1001 1002
 1001 1002 1003
 1002 1003 1004
 1003 1004 1005
 1004 1005 1006
 1005 1006 1007
 1006 1007 1008
 1007 1008 1009
 1008 1009 1010
 1009 1010 1011
 1010 1011 1012
 1011 1012 1013
 1012 1013 1014
 1013 1014 1015
 1014 1015 1016
 1015 1016 1017
 1016 1017 1018
 1017 1018 1019
 1018 1019 1020
 1019 1020 1021
 1020 1021 1022
 1021 1022 1023
 1022 1023 1024
 1023 1024 1025
 1024 1025 1026
 1025 1026 1027
 1026 1027 1028
 1027 1028 1029
 1028 1029 1030
 1029 1030 1031
 1030 1031 1032
 1031 1032 1033
 1032 1033 1034
 1033 1034 1035
 1034 1035 1036
 1035 1036 1037
 1036 1037 1038
 1037 1038 1039
 1038 1039 1040
 1039 1040 1041
 1040 1041 1042
 1041 1042 1043
 1042 1043 1044
 1043 1044 1045
 1044 1045 1046
 1045 1046 1047
 1046 1047 1048
 1047 1048 1049
 1048 1049 1050
 1049 1050 1051
 1050 1051 1052
 1051 1052 1053
 1052 1053 1054
 1053 1054 1055
 1054 1055 1056
 1055 1056 1057
 1056 1057 1058
 1057 1058 1059
 1058 1059 1060
 1059 1060 1061
 1060 1061 1062
 1061 1062 1063
 1062 1063 1064
 1063 1064 1065
 1064 1065 1066
 1065 1066 1067
 1066 1067 1068
 1067 1068 1069
 1068 1069 1070
 1069 1070 1071
 1070 1071 1072
 1071 1072 1073
 1072 1073 1074
 1073 1074 1075
 1074 1075 1076
 1075 1076 1077
 1076 1077 1078
 1077 1078 1079
 1078 1079 1080
 1079 1080 108

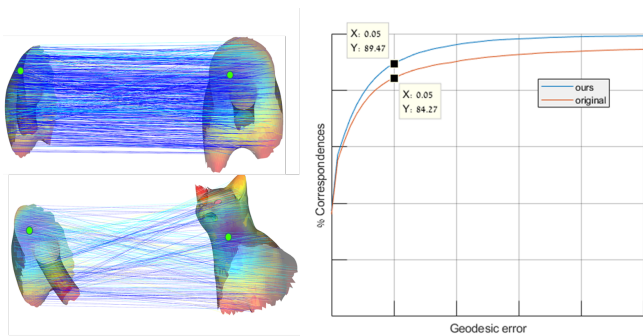


Figure 3. Qualitative and quantitative illustration of the improvement introduced by our formulation. On the top left the Nearest neighbor mapping between the part and its corresponding ground truth geodesic disc. As can be seen low distortion is occurring between the true corresponding points, but the symmetrical part which is not included on the partial model maps to the same points - thus attenuating the score originating from these. One the bottom left we see the piece chosen by the original DDIS formulation. The arrows with low distortion seldom have other points which are their nearest neighbors and thus achieves a better score without our modification. The cumulative error curves show an improvement of 5 percent on the training set using our formulation.

Overview We'll first give an overview, and then give an extended description of each of each stage.

We start by calculating the normals for \mathcal{M} and \mathcal{N} . We then calculate local point descriptors for each patch of some neighborhood around the points in each mesh (For our purpose FPFH seemed to work the best of our tested descriptors). Having calculated these, we calculate a nearest neighbor field by finding for each patch in \mathcal{M} it's Nearest Neighbor in \mathcal{N} . We now find the distance of every point $n \in \mathcal{N}$ to the desired point $y \in \mathcal{N}$ for a desired neighborhood R_T . We now go over every point $x \in \mathcal{M}$. For each we extract the geodesic disc \mathcal{M}_{x,R_T} around it. We take notice that while the above stages are done here in the context of template matching for one template, when matching multiple templates all of the above calculations have to be done only once between the shapes, with the exception of geodesic distance field extraction for the template itself. Finally we calculate DDIS for this disc with $\mathcal{N}_{y,R}$ which has y as it's center. Having done that for every point, the point $y^* \in \mathcal{M}$ which gets the maximal DDIS Score is deemed the corresponding point to y .

Point Normal Estimation There are various schemes for estimating point normals given a triangulated mesh surface. We have picked the one which is available in the standard PCL. Given a vertex p_i on a triangulated mesh \mathcal{X} and it's associated polygons $\{A_j\}_{j=1}^k$ and their normals N_{A_j} the point normal $N_i = \sum_{j=1}^k |A_j| \cdot N_{A_j}$

Local Patch Descriptor DDIS as defined by [30] uses patch descriptors as low level features for their similarity

measure. While a patch in an image can be defined by the images grid no such grid exists on 3D point clouds and meshes, where density of data points can vary. Thus a patch has to be defined by some geometric measure. While the more robust way to define it would be using geodesic distance, since we are talking a small environment around a point on the mesh we have found that for practical purposes a patch in a defined euclidean radius r_F around a point serves well enough. We pick this radius in the following way: given the full surface mesh \mathcal{M} we find it's equivalent of a diameter $D_{\mathcal{M}} = \sqrt{\text{Area}(\mathcal{M})}$, and tune a parameter α to obtain $r_F = \frac{\alpha}{*} D_{\mathcal{M}}$. A lot of local shape descriptors have been used successfully in 3D shape analysis. We have tested the following descriptors: PFH[24] SHOT[31], HKS[?], SIHKS[7], ROPS[?] and FPFH[23]. Out of these FPFH has achieved the best performance, and thus the descriptor for the local patch has been chosen to be FPFH.

Nearest Neighbor Field As an intermediate stage towards the calculation of Deformable Diversity Similarity measure, the calculation of the nearest neighbor field (will be abbreviated as NNF) needs to be calculated. Thus for every patch $m \in \mathcal{M}$ we have to find the patch on the template $n \in \mathcal{N}$ which resembles it the most. For FPFH, $NN^S(m_j, \mathcal{N})$ is defined $NN^S(m_j, \mathcal{N}) \equiv \underset{i}{\operatorname{argmin}} \chi^2(FPFH(m_j], FPFH(n_i))$ and the Nearest Neighbor Field is the set of all these correspondences.

DDIS calculation For every point in $m_x \in \mathcal{M}$ we then extract a geodesic disk $\mathcal{M}_{x,R}$ with a radius R_T around it and calculate deformable diversity score for it. The point which maximizes the similarity score gives us a correspondence $(y, y^*) \in \mathcal{N} \times \mathcal{M}$.

4.2. DDIS Sparse Correspondences

A key takeaway from experimenting with DDIS as a template matching algorithm for partial matching has been that isometry does not hold, at least not globally. It does however, hold pretty well locally, especially at extremities. To this end we devise multiple template matching framework for Partial correspondences of deformable shapes. We first obtain landmarks $F_{init} = \{f\}_i$ as described in [1]. We then employ a simple sampling scheme which ensures a good quasi uniform covering of the surface. Finally, we for each sample point we extract a geodesic disc, and find its counterpart on \mathcal{M} which maximizes DDIS.

Landmark Extraction We follow the work of [?] to obtain mesh extremities. Given a shape the work employs the following framework to extract it's extremities. A point is detected as an extremity if it fulfills 2 conditions: - it's sum of geodesic distances is a local extrema, formally, for $v \in S$, where S is a surface mesh, we define the set of points with

756 a direct edge to it as N_v , the point is a critical point if :

$$\sum_{v_i \in S} d_{geo}(v, v_i) > \sum_{v_i \in S} d_{geo}(v_n, v_i), \forall v_n \in N_v \quad (7)$$

757 An additional requirement for it to be an extremities is for
 758 it to lie on the convex hull of the shape's MDS. In this work
 759 we have dropped the last condition, but chose N_v* - a neighbor-
 760 hood of $0.03 \cdot \sqrt{Area(S)}$. This stage gives us the initial
 761 set of sample denoted S_0

762 **Mesh sampling** We employ a sampling
 763 scheme very reminiscent of the one employed
 764 in [glu2011coarse]. In each stage k , we take the set of samples S_{k-1} and mark all the points
 765 in a radius R_S around them. From the set of remaining
 766 point we choose the one whose distance to the set S_{k-1} is
 767 minimal to create the set S_k . We repeat this process until
 768 all the points are marked.

769 **Algorithm 1** 3DIS Sparse Correspondences

```

770 procedure DDIS CORRESPONDENCE( $\mathcal{M}, \mathcal{N}, \alpha, \beta, \gamma$ )  $\triangleright$ 
771     Returns point correspondence for critical points on  $\mathcal{N}$ 
772
773      $r_F \leftarrow \alpha/100 \cdot \sqrt{Area(\mathcal{M})}$ 
774      $R_{thresh} \leftarrow \beta/100 \cdot \sqrt{Area(\mathcal{M})}$ 
775      $N_{\mathcal{M}} \leftarrow ComputeNormals(\mathcal{M})$ 
776      $N_{\mathcal{N}} \leftarrow ComputeNormals(\mathcal{N})$ 
777      $F_{\mathcal{M}} \leftarrow FPFH(\mathcal{M}, N_{\mathcal{M}}, r_F)$ 
778      $F_{\mathcal{N}} \leftarrow FPFH(\mathcal{N}, N_{\mathcal{N}}, r_F)$ 
779      $NNF_{\mathcal{M} \rightarrow \mathcal{N}} \leftarrow ANN(F_{\mathcal{M}}, F_{\mathcal{N}})$ 
780      $\mathcal{N}_c = \{n : \sum_{n_i \in \mathcal{N}} d_{geo}(n, n_i) >$ 
781      $\sum_{n_i \in \mathcal{N}} d_{geo}(n_N, n_i), \forall n_N : d_{geo}(n, n_N) <$ 
782      $0.03 \cdot \sqrt{Area(\mathcal{M})}\}$ 
783     for  $n_y \in \mathcal{N}_c$  do  $\triangleright$  DDIS calculation Loop
784          $m_c* \leftarrow DDIS\_Correspondence(\mathcal{M}, n_y, \mathcal{N}, \alpha, \beta, \gamma)$ 
785     end for
786     return  $\mathcal{M}_c \times \mathcal{N}_c = \{m_c*, n_c\}$ 
787 end procedure

```

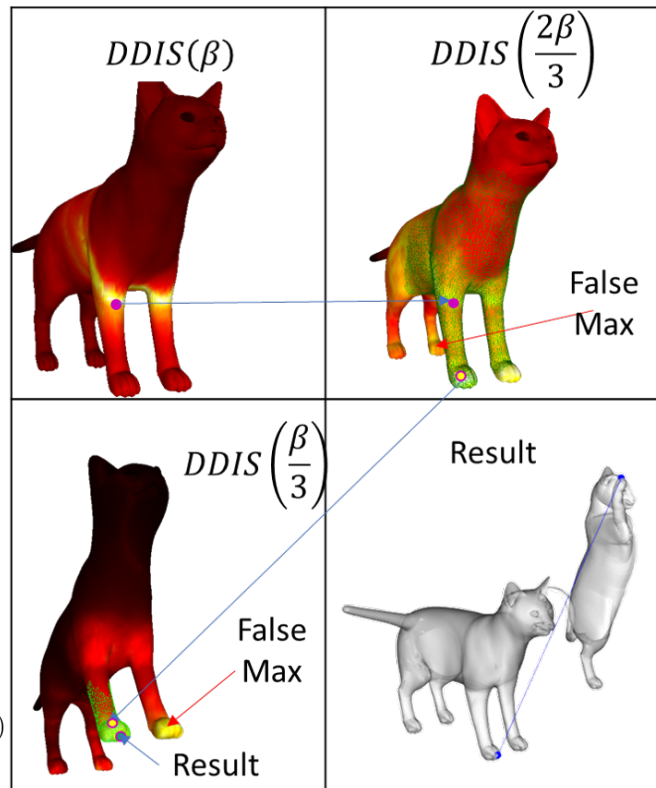
788 **Landmark Template Matching** For this end, we create
 789 a template for each landmark point - we collect all surface
 790 point in a surrounding geodesic disc of radius $R_T =$
 791 $\beta \cdot \sqrt{Area(\mathcal{M})}$. While it might seem natural to calculate a
 792 different nearest neighbor field for each landmark template
 793 it has been empirically found that using the global nearest
 794 neighbor field gives much better results. This is hypothe-
 795 sized to occur due to the fact that this nearest neighbor
 796 field encodes global information when obtained this way
 797 and might eliminates local distractors.

798 Each landmark template is compared to all surface parts
 799 of a similar R_T on \mathcal{M} to obtain correspondences.

800 **4.3. Cascaded Multi-Scale DDIS**

801 The observation of the effects of the choice of β and the
 802 trade-off between finer localization and avoidance of global

803 errors naturally leads to the adoption of a multi scale frame-
 804 work. We calculate *DDIS* score for multiple β values,
 805 and use the location obtained with a large β to select a
 806 narrow environment in which we look for the maximum
 807 of *DDIS* with a smaller value β , thus using the larger
 808 scale to get a rough global location, and the smaller scale
 809 to fit it into a more exact location. While this might be
 810 done at multiple custom scales we have found that the triplet
 811 $\beta, 2 \cdot \beta/3, 3\beta/3$ works well.



812 Figure 4. Illustration of the multi scale framework. The green grid
 813 marks the area chosen by the previous scale to be valid. It can be
 814 seen that wrong maxima in lower scales are ignored due to this
 815 process

816 **4.4. Greedy Outlier Fix**

817 The results obtained by the pipeline, while empiri-
 818 cally already producing matches of superior quality to
 819 state of the art algorithms in the field nevertheless have
 820 no explicit requirement on generating a coherent set of
 821 matches. We thus as a post processing step identify
 822 outliers and replace them with more suitable corre-
 823 spondences. Inspired by distortion minimization methods such
 824 as [glu2011coarse, glu2011coarse] we pick the distortion of
 825 a correspondence as a measure of its coherency to the
 826 set. For a correspondence $(y, x) \in \mathcal{N} \times \mathcal{M}$ the distor-
 827 tion as the mean of its deviation of relative distance to all

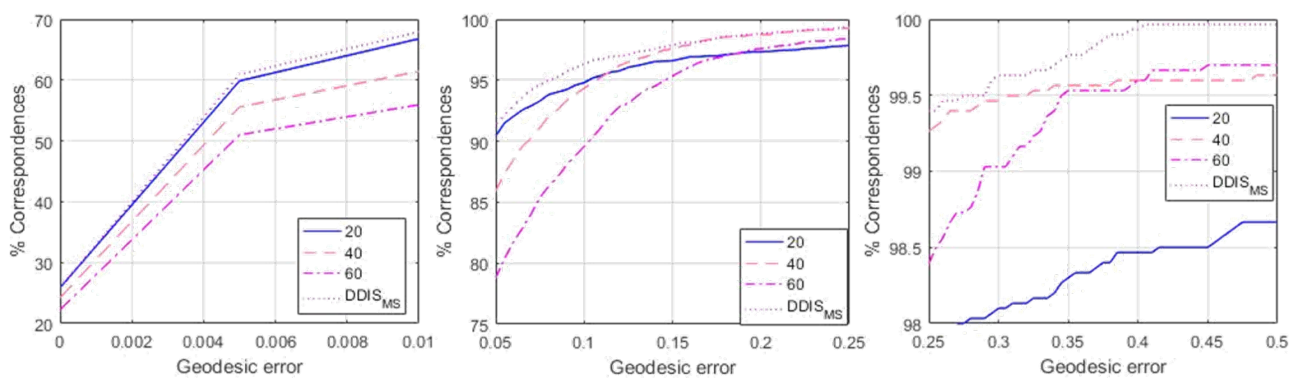


Figure 5. Effect of the β parameter on the results: it can be seen that a smaller beta promotes better localization in a small neighborhood, while higher values of β lead to more local errors but are more robust to global errors. It can be seen that the multi-scale cascade achieves better results both locally and globally.

other points in the set. Given a set of correspondences $P = p_i = (y_i, x_i) \in \mathcal{N} \times \mathcal{M}$ the distortion is defined by the equation

$$D(p_i) = \frac{1}{|P| - 1} \sum_{j \neq i} \rho(p_i, p_j) \quad (8)$$

where ρ is the individual relative distortion induced by 2 correspondences

$$\rho(p_i, p_j) = \max\left(\frac{d(y_i, y_j)}{d(x_i, x_j)}, \frac{d(x_i, x_j)}{d(y_i, y_j)}\right) \quad (9)$$

where d is the geodesic distance between 2 points. We first filter out outliers by thresholding matches whose distortion is larger than 1.2 of the mean distortion, and then greedily add from the set of DDIS maximas the point which minimizes this distortion.

4.5. Densification

If necessary, the sparse correspondences produced by our algorithm can then be passed as an input for the method of [14] to produce dense matches. This is done in a manner identical to the refinement step which is already used in the method, and improves its results.

5. Experiments and results

In this section we will briefly go over the experiments performed and their results. We'll introduce the datasets, detail our experiments and their results

5.1. Datasets

In this section we will briefly go over the available Datasets

5.1.1 SHREC 2016

The SHREC partial matching dataset consists of 8 base, neutral pose models: cat, centaur, dog, horse, wolf, and 3 humans – 2 males, and 1 female. Each basic model has corresponding deformed partial shapes obtained either by cutting the shape with a plane or by adding holes on a deformed shape. The set has been divided into train and test sets. The train set is composed of 15 cuts for each base models totaling 120 models, and 10 holed shapes for each model for which ground truth point to polygon correspondences has been provided in barycentric coordinates. The test set is composed of additional 200 cuts and 200 holed shapes.

5.2. Error Metrics

The output of partial matching algorithms (as defined in [8]) are sub-vertex point-to-point correspondences between partial shapes. For all experiments we use the standard practice of not penalizing symmetric solutions. Quality is measured according to the Princeton benchmark protocol [11]. For a pair of points $(x, y) \in \mathcal{N} \times \mathcal{M}$ between the full object \mathcal{M} and the partial shape \mathcal{N} produced by an algorithm, where (x, y^*) is the ground truth correspondence the inaccuracy is measured by

$$\varepsilon(x) = \frac{d_{\mathcal{M}}(y, y^*)}{\sqrt{\text{area}(\mathcal{M})}} \quad (10)$$

where $d_{\mathcal{M}}(y, y^*)$ is the geodesic distance on \mathcal{M} , and has units of normalized length on \mathcal{M} . For dense correspondences over a dataset, $\varepsilon(x)$ is averaged over all matching instances.

5.2.1 Central Points Localization

In this experiment we have chosen for each Template mesh the center point c_T and tried to match it to a point on the ob-

972 ject using DDIS. Experiments have been done using FPFH,
 973 PFH and SHOT as patch descriptors with patch radiiuses of
 974 [2, 3, 4, 5], the results of the opimal parameter for each de-
 975 scriptor are illustrated in fig. and visualizations of similarity
 976 maps of cuts are provided in fig. . It can be seen that
 977 good localization is obtained for points on a smooth sur-
 978 face, under high partiality conditions and strong deforma-
 979 tions. Bad matches occur when a matched point resides on
 980 a heavily deformed patch, and when salient anchor points
 981 are deformed or cut. Analysis of these results shows a drift
 982 in localization occurs when salient features are divided by
 983 strong unisometric deformations which serve as the motiva-
 984 tion for the multiple template matching framework.
 985

987 5.3. Sparse Correspondences on the SHREC16 Test 988 set

990 In this experiment we have tested the performance
 991 of DDIS in producing sparse correspondences on the
 992 SHREC16 Partial Matching of Deformable Shapes compe-
 993 tition. We had tuned our parameters on the SHREC16 train-
 994 ing dataset using only the cuts part of it. The best results had
 995 been produced using FPFH with $r_F = 0.03\sqrt{\text{Area}(\mathcal{M})}$,
 996 and a piece size radii of $R_T = [0.6, 0.4, 0.2]\sqrt{\text{Area}(\mathcal{M})}$.
 997 For Geodesic distances we have found the fast marching al-
 998 gorithm to work the fastest, while giving the lowest error
 999 w.r.t. to exact geodesics. For a 10,000 vertices mesh it takes
 1000 60s to produce a full distance matrix, Though it should be
 1001 noted this algorithm has a more efficient GPU implemen-
 1002 tation, and parallelization on a core brought the run time to
 1003 12s with 6 threads. FPFH and Nearest Neighbor field takes
 1004 2s, and similarity between 2 pieces of 10000 vertices each
 1005 takes XXs on average, running on 6 threads of i7-2700k.
 1006 Unlike optimization based algorithms this is highly paral-
 1007 lelizable. We achieve results comparable to the state of the
 1008 art [14] quality wise, even though sparser in nature on both
 1009 the Cuts and the Holes datasets, Where a particularly im-
 1010 pressive result is reported on the Holes dataset, which can
 1011 then be expanded without a loss of quality by feeding these
 1012 to the FSPM[14] as input instead of low level shape descrip-
 1013 tors.
 1014

	PFM	RF	IM	EN	GT	DDIS
cuts	dense	dense	61.3	87.8	51.0	132.2
holes	dense	dense	78.2	112.6	76.4	77.3

1015 Table 1. mean number of correspondence obtained by the algo-
 1016 rithms in the SHREC 16 competiton and our algorithm
 1017

1018
 1019
 1020
 1021
 1022
 1023
 1024
 1025
 glu2011coarseggglu2011coarse,
 lu2011coarseglu2011coarseggglu2011coarse,
 lu2011coarseglu2011coarseggglu2011coarse,
 lu2011coarseglu2011coarseggglu2011coarse,

References

- [1] D. Aiger, N. J. Mitra, and D. Cohen-Or. 4pointss congruent sets for robust pairwise surface registration. *ACM Trans. Graph.*, 27(3):85:1–85:10, Aug. 2008. 3
- [2] M. Aubry, U. Schlickewei, and D. Cremers. The wave kernel signature: A quantum mechanical approach to shape analysis. In *Computer Vision Workshops (ICCV Workshops), 2011 IEEE International Conference on*, pages 1626–1633. IEEE, 2011. 3
- [3] D. Boscaini, J. Masci, E. Rodolà, and M. Bronstein. Learning shape correspondence with anisotropic convolutional neural networks. In *Advances in Neural Information Processing Systems*, pages 3189–3197, 2016. 3
- [4] A. M. Bronstein and M. M. Bronstein. Not only size matters: regularized partial matching of nonrigid shapes. In *Computer Vision and Pattern Recognition Workshops, 2008. CVPRW’08. IEEE Computer Society Conference on*, pages 1–6. IEEE, 2008. 2, 3
- [5] A. M. Bronstein, M. M. Bronstein, A. M. Bruckstein, and R. Kimmel. Partial similarity of objects, or how to compare a centaur to a horse. *International Journal of Computer Vision*, 84(2):163, 2009. 3
- [6] A. M. Bronstein, M. M. Bronstein, and R. Kimmel. Generalized multidimensional scaling: a framework for isometry-invariant partial surface matching. *Proceedings of the National Academy of Sciences*, 103(5):1168–1172, 2006. 2, 3
- [7] M. M. Bronstein and I. Kokkinos. Scale-invariant heat kernel signatures for non-rigid shape recognition. In *Computer Vision and Pattern Recognition (CVPR), 2010 IEEE Conference on*, pages 1704–1711. IEEE, 2010. 3, 7
- [8] L. Cosmo, E. Rodolà, M. Bronstein, A. Torsello, D. Cremers, and Y. Sahillioglu. Shrec’16: Partial matching of deformable shapes. *Proc. 3DOR*, 2, 2016. 2, 9
- [9] T. Dekel, S. Oron, M. Rubinstein, S. Avidan, and W. T. Freeman. Best-buddies similarity for robust template matching. In *Proceedings of the IEEE Conference on Computer Vision and Pattern Recognition*, pages 2021–2029, 2015. 4
- [10] D. Holz, A. E. Ichim, F. Tombari, R. B. Rusu, and S. Behnke. Registration with the point cloud library: A modular framework for aligning in 3-d. *IEEE Robotics & Automation Magazine*, 22(4):110–124, 2015. 2
- [11] V. G. Kim, Y. Lipman, and T. Funkhouser. Blended intrinsic maps. In *ACM Transactions on Graphics (TOG)*, volume 30, page 79. ACM, 2011. 9
- [12] A. Kovnatsky, M. M. Bronstein, X. Bresson, and P. Vandergheynst. Functional correspondence by matrix completion. In *Proceedings of the IEEE conference on computer vision and pattern recognition*, pages 905–914, 2015. 3
- [13] Y. Lipman and T. Funkhouser. Möbius voting for surface correspondence. *ACM Transactions on Graphics (TOG)*, 28(3):72, 2009. 3
- [14] O. Litany, E. Rodolà, A. M. Bronstein, and M. M. Bronstein. Fully spectral partial shape matching. In *Computer Graphics Forum*, volume 36, pages 247–258. Wiley Online Library, 2017. 2, 3, 9, 10

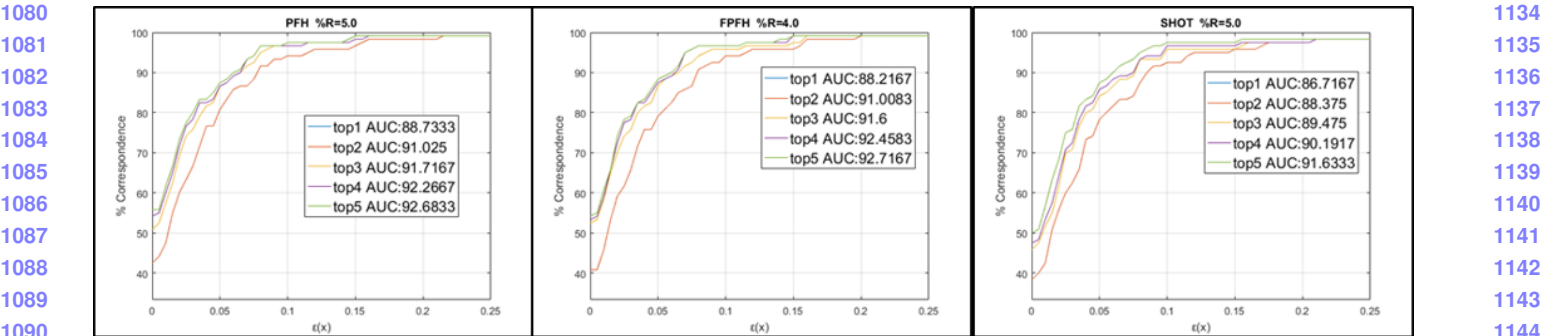


Figure 6. Comparison between descriptors: we show curves for the minimal distance of the top results. a noticeable addition occurs when adding the 2nd best match

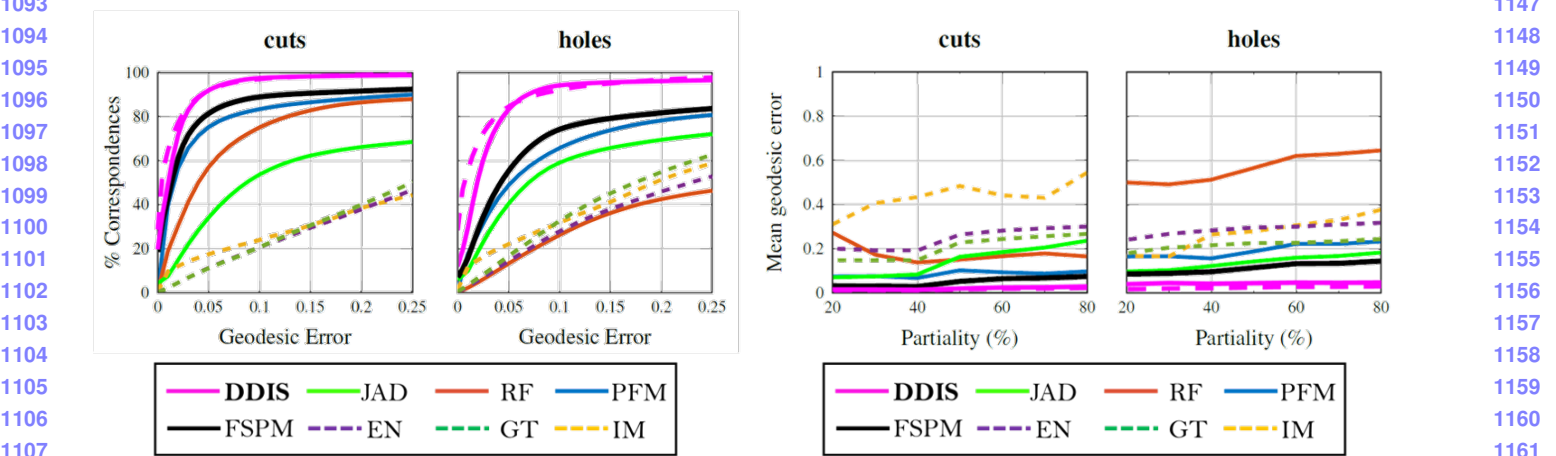


Figure 7. comparison with other state of the art algorithms - it can be seen that although sparse in nature, the correspondence obtained by DDIS are much more accurate than the other methods. A separate analysis has been done for correspondences which include boundary points, which tend to be more noisy, and internal points which are more sparse

- [15] J. Masci, E. Rodolà, D. Boscaini, M. M. Bronstein, and H. Li. Geometric deep learning. In *SIGGRAPH ASIA 2016 Courses*, page 1. ACM, 2016. 3
- [16] F. Monti, D. Boscaini, and J. Masci. Geometric deep learning on graphs and manifolds using mixture model cnns. 3
- [17] M. Ovsjanikov, M. Ben-Chen, J. Solomon, A. Butscher, and L. Guibas. Functional maps: A flexible representation of maps between shapes. *ACM Trans. Graph.*, 31(4):30:1–30:11, July 2012. 2, 3
- [18] J. Pokrass, A. M. Bronstein, and M. M. Bronstein. Partial shape matching without point-wise correspondence. *Numerical Mathematics: Theory, Methods and Applications*, 6(1):223–244, 2013. 3
- [19] J. Pokrass, A. M. Bronstein, M. M. Bronstein, P. Sprechmann, and G. Sapiro. Sparse modeling of intrinsic correspondences. In *Computer Graphics Forum*, volume 32, pages 459–468. Wiley Online Library, 2013. 3
- [20] E. Rodolà, S. R. Bulò, T. Windheuser, M. Vestner, and D. Cremers. Dense non-rigid shape correspondence using random forests. In *Proceedings of the 2014 IEEE Conference on Computer Vision and Pattern Recognition, CVPR ’14*, pages 4177–4184, Washington, DC, USA, 2014. IEEE Computer Society. 3

- [21] E. Rodolà, L. Cosmo, M. M. Bronstein, A. Torsello, and D. Cremers. Partial functional correspondence. In *Computer Graphics Forum*, volume 36, pages 222–236. Wiley Online Library, 2017. 2, 3
- [22] E. Rodolà, A. Torsello, T. Harada, Y. Kuniyoshi, and D. Cremers. Elastic net constraints for shape matching. In *Proceedings of the IEEE International Conference on Computer Vision*, pages 1169–1176, 2013. 3
- [23] R. B. Rusu, N. Blodow, and M. Beetz. Fast point feature histograms (fpfh) for 3d registration. In *Robotics and Automation, 2009. ICRA’09. IEEE International Conference on*, pages 3212–3217. Citeseer, 2009. 2, 3, 7
- [24] R. B. Rusu, Z. C. Marton, N. Blodow, and M. Beetz. Learning informative point classes for the acquisition of object model maps. In *Control, Automation, Robotics and Vision, 2008. ICARCV 2008. 10th International Conference on*, pages 643–650. IEEE, 2008. 3, 7
- [25] R. B. Rusu, Z. C. Marton, N. Blodow, M. Dolha, and M. Beetz. Towards 3d point cloud based object maps for household environments. *Robotics and Autonomous Systems*, 56(11):927–941, 2008. 3
- [26] Y. Sahillioglu and Y. Yemez. Minimum-distortion isometric shape correspondence using em algorithm. *IEEE*

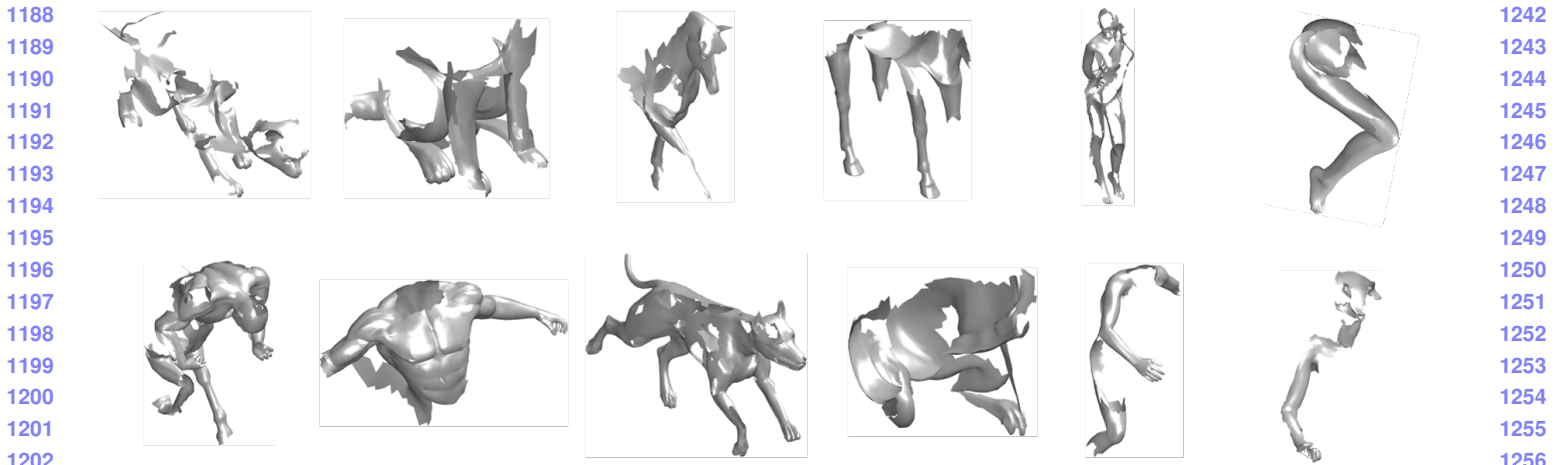


Figure 8. SHREC 16 holes partial matching dataset.

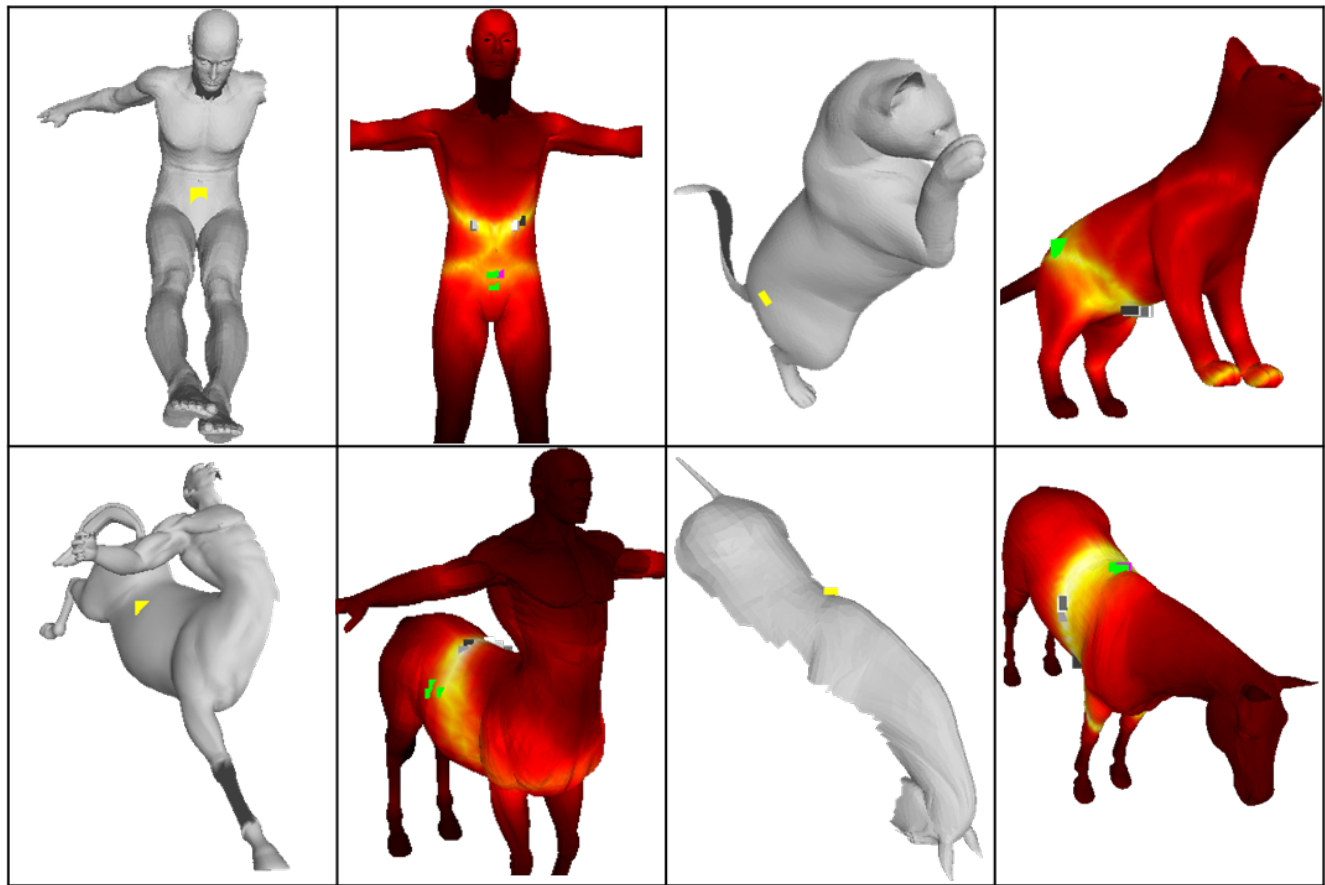


Figure 9. Some notable failure cases

transactions on pattern analysis and machine intelligence, 34(11):2203–2215, 2012. 3

- [27] Y. Sahillioğlu and Y. Yemez. Scale normalization for isometric shape matching. In *Computer Graphics Forum*, volume 31, pages 2233–2240. Wiley Online Library, 2012. 3
- [28] Y. Sahillioğlu and Y. Yemez. Coarse-to-fine combinatorial matching for dense isometric shape cor-
- respondence. In *Computer Graphics Forum*, volume 30, pages 1461–1470. Wiley Online Library, 2011. ■ğlu2011coarse0■ğlu2011coarse0ğlu2011coarse
- [29] A. Shtern and R. Kimmel. Matching the lbo eigenspace of non-rigid shapes via high order statistics. *Axioms*, 3(3):300–319, 2014. 3
- [30] I. Talmi, R. Mechrez, and L. Zelnik-Manor. Template match-

- 1296 ing with deformable diversity similarity. In *Proc. of IEEE*
 1297 *Conf. on Computer Vision and Pattern Recognition*, pages
 1298 1311–1319, 2017. 2, 4, 7
- 1299 [31] F. Tombari, S. Salti, and L. Di Stefano. Unique signatures of
 1300 histograms for local surface description. In *European conference on computer vision*, pages 356–369. Springer, 2010. 3, 7
- 1301 [32] A. Torsello. A game-theoretic approach to deformable shape
 1302 matching. In *Proceedings of the 2012 IEEE Conference on Computer Vision and Pattern Recognition (CVPR)*, CVPR ’12, pages 182–189, Washington, DC, USA, 2012. IEEE Computer Society. 2, 3
- 1303 [33] M. Vestner, Z. Lähner, A. Boyarski, O. Litany, R. Slossberg,
 1304 T. Remez, E. Rodola, A. Bronstein, M. Bronstein, R. Kimmel, et al. Efficient deformable shape correspondence via
 1305 kernel matching. In *3D Vision (3DV), 2017 International Conference on*, pages 517–526. IEEE, 2017. 2, 3
- 1306 [34] **References**
- 1307 [1] D. Aiger, N. J. Mitra, and D. Cohen-Or. 4pointss congruent sets for robust pairwise surface registration. *ACM Trans. Graph.*, 27(3):85:1–85:10, Aug. 2008. 3
- 1308 [2] M. Aubry, U. Schlickewei, and D. Cremers. The wave kernel
 1309 signature: A quantum mechanical approach to shape analy-
 1310 sis. In *Computer Vision Workshops (ICCV Workshops), 2011 IEEE International Conference on*, pages 1626–1633. IEEE, 2011. 3
- 1311 [3] D. Boscaini, J. Masci, E. Rodolà, and M. Bronstein. Learning shape correspondence with anisotropic convolutional
 1312 neural networks. In *Advances in Neural Information Processing Systems*, pages 3189–3197, 2016. 3
- 1313 [4] A. M. Bronstein and M. M. Bronstein. Not only size mat-
 1314 ters: regularized partial matching of nonrigid shapes. In *Computer Vision and Pattern Recognition Workshops, 2008. CVPRW’08. IEEE Computer Society Conference on*, pages 1–6. IEEE, 2008. 2, 3
- 1315 [5] A. M. Bronstein, M. M. Bronstein, A. M. Bruckstein, and
 1316 R. Kimmel. Partial similarity of objects, or how to compare a
 1317 centaur to a horse. *International Journal of Computer Vision*,
 1318 84(2):163, 2009. 3
- 1319 [6] A. M. Bronstein, M. M. Bronstein, and R. Kimmel. Generalized multidimensional scaling: a framework for isometry-
 1320 invariant partial surface matching. *Proceedings of the National Academy of Sciences*, 103(5):1168–1172, 2006. 2, 3
- 1321 [7] M. M. Bronstein and I. Kokkinos. Scale-invariant heat ker-
 1322 nel signatures for non-rigid shape recognition. In *Computer Vision and Pattern Recognition (CVPR), 2010 IEEE Conference on*, pages 1704–1711. IEEE, 2010. 3, 7
- 1323 [8] L. Cosmo, E. Rodolà, M. Bronstein, A. Torsello, D. Cremers,
 1324 and Y. Sahillioglu. Shrec’16: Partial matching of deformable
 1325 shapes. *Proc. 3DOR*, 2, 2016. 2, 9
- 1326 [9] T. Dekel, S. Oron, M. Rubinstein, S. Avidan, and W. T. Free-
 1327 man. Best-buddies similarity for robust template matching.
 1328 In *Proceedings of the IEEE Conference on Computer Vision and Pattern Recognition*, pages 2021–2029, 2015. 4
- 1329 [10] D. Holz, A. E. Ichim, F. Tombari, R. B. Rusu, and S. Behnke. Registration with the point cloud library: A modular frame-
 1330 work for aligning in 3-d. *IEEE Robotics & Automation Magazine*, 22(4):110–124, 2015. 2
- 1331 [11] V. G. Kim, Y. Lipman, and T. Funkhouser. Blended intrinsic
 1332 maps. In *ACM Transactions on Graphics (TOG)*, volume 30, page 79. ACM, 2011. 9
- 1333 [12] A. Kovnatsky, M. M. Bronstein, X. Bresson, and P. Vand-
 1334 ergheynst. Functional correspondence by matrix comple-
 1335 tion. In *Proceedings of the IEEE conference on computer vision and pattern recognition*, pages 905–914, 2015. 3
- 1336 [13] Y. Lipman and T. Funkhouser. Möbius voting for surface
 1337 correspondence. *ACM Transactions on Graphics (TOG)*, 28(3):72, 2009. 3
- 1338 [14] O. Litany, E. Rodolà, A. M. Bronstein, and M. M. Bronstein. Fully spectral partial shape matching. In *Computer Graphics Forum*, volume 36, pages 247–258. Wiley Online Library, 2017. 2, 3, 9, 10
- 1339 [15] J. Masci, E. Rodolà, D. Boscaini, M. M. Bronstein, and H. Li. Geometric deep learning. In *SIGGRAPH ASIA 2016 Courses*, page 1. ACM, 2016. 3
- 1340 [16] F. Monti, D. Boscaini, and J. Masci. Geometric deep learning
 1341 on graphs and manifolds using mixture model cnns. 3
- 1342 [17] M. Ovsjanikov, M. Ben-Chen, J. Solomon, A. Butscher, and L. Guibas. Functional maps: A flexible representation of
 1343 maps between shapes. *ACM Trans. Graph.*, 31(4):30:1–30:11, July 2012. 2, 3
- 1344 [18] J. Pokrass, A. M. Bronstein, and M. M. Bronstein. Partial
 1345 shape matching without point-wise correspondence. *Numerical Mathematics: Theory, Methods and Applications*, 6(1):223–244, 2013. 3
- 1346 [19] J. Pokrass, A. M. Bronstein, M. M. Bronstein, P. Sprech-
 1347 mann, and G. Sapiro. Sparse modeling of intrinsic cor-
 1348 respondences. In *Computer Graphics Forum*, volume 32, pages 459–468. Wiley Online Library, 2013. 3
- 1349 [20] E. Rodolà, S. R. Bulò, T. Windheuser, M. Vestner, and D. Cremers. Dense non-rigid shape correspondence using
 1350 random forests. In *Proceedings of the 2014 IEEE Conference on Computer Vision and Pattern Recognition*, CVPR ’14, pages 4177–4184, Washington, DC, USA, 2014. IEEE Computer Society. 3
- 1351 [21] E. Rodolà, L. Cosmo, M. M. Bronstein, A. Torsello, and D. Cremers. Partial functional correspondence. In *Computer Graphics Forum*, volume 36, pages 222–236. Wiley Online Library, 2017. 2, 3
- 1352 [22] E. Rodolà, A. Torsello, T. Harada, Y. Kuniyoshi, and D. Cremers. Elastic net constraints for shape matching. In *Proceedings of the IEEE International Conference on Computer Vision*, pages 1169–1176, 2013. 3
- 1353 [23] R. B. Rusu, N. Blodow, and M. Beetz. Fast point feature
 1354 histograms (fpfh) for 3d registration. In *Robotics and Au-
 1355 tomation, 2009. ICRA’09. IEEE International Conference on*, pages 3212–3217. Citeseer, 2009. 2, 3, 7
- 1356 [24] R. B. Rusu, Z. C. Marton, N. Blodow, and M. Beetz. Learn-
 1357 ing informative point classes for the acquisition of object
 1358 model maps. In *Control, Automation, Robotics and Vi-
 1359 sion, 2008. ICARCV 2008. 10th International Conference on*, pages 643–650. IEEE, 2008. 3, 7

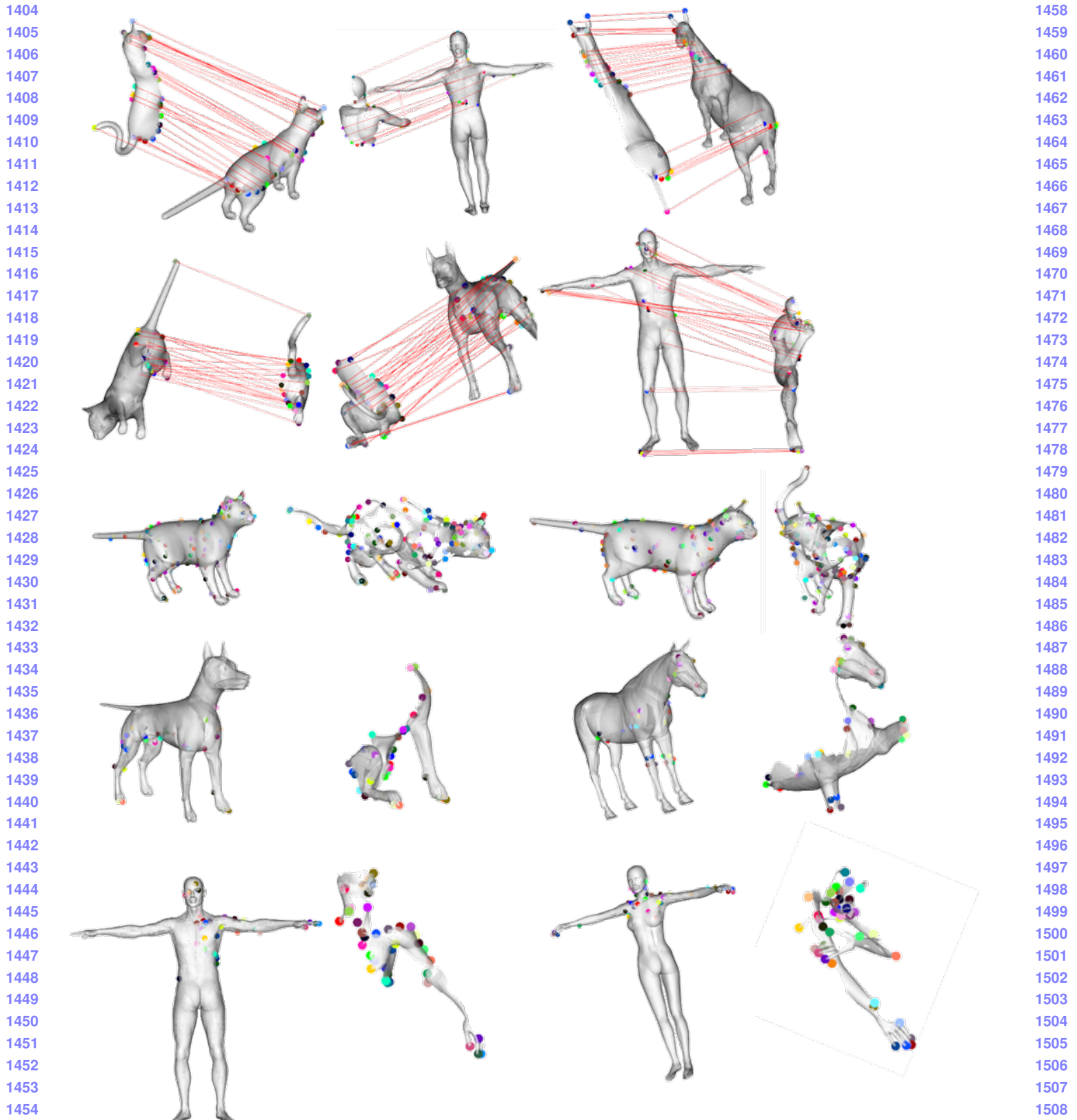


Figure 10. Good correspondences obtained by our method

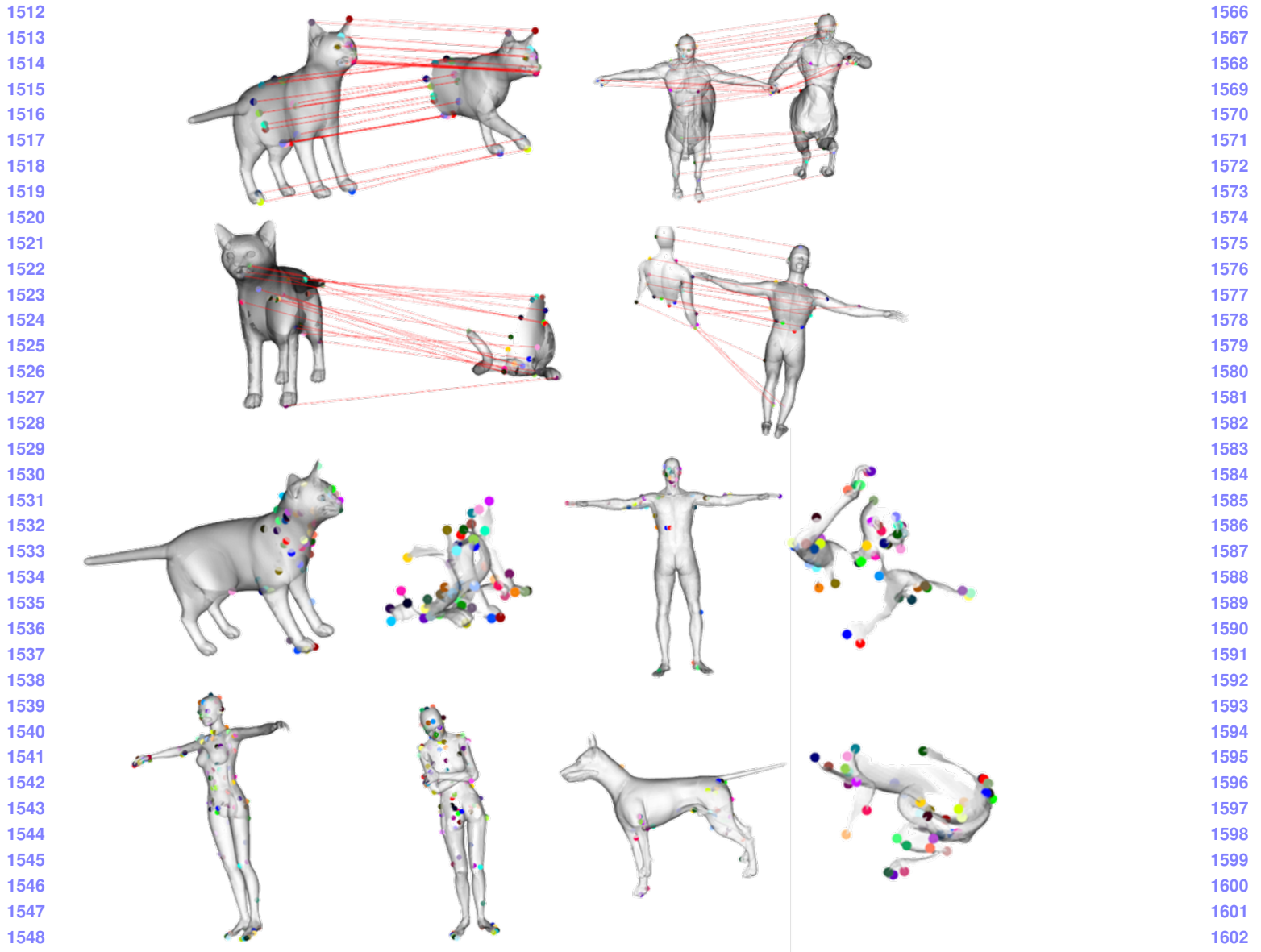


Figure 11. Some notable failure cases - most common is cat paw assignment - an extrinsic near symmetry gives rise to this phenomena. Closed fists on humanoids tends to cause a collapse of all fingers to a single finger. In the holes extreme partiality makes the geodesic distances break even over short distances.

- [25] R. B. Rusu, Z. C. Marton, N. Blodow, M. Dolha, and M. Beetz. Towards 3d point cloud based object maps for household environments. *Robotics and Autonomous Systems*, 56(11):927–941, 2008. 3
- [26] Y. Sahillioğlu and Y. Yemez. Minimum-distortion isometric shape correspondence using em algorithm. *IEEE transactions on pattern analysis and machine intelligence*, 34(11):2203–2215, 2012. 3
- [27] Y. Sahillioğlu and Y. Yemez. Scale normalization for isometric shape matching. In *Computer Graphics Forum*, volume 31, pages 2233–2240. Wiley Online Library, 2012. 3
- [28] Y. Sahillioğlu and Y. Yemez. Coarse-to-fine combinatorial matching for dense isometric shape correspondence. In *Computer Graphics Forum*, volume 30, pages 1461–1470. Wiley Online Library, 2011. 3
- [29] A. Shtern and R. Kimmel. Matching the lbo eigenspace of non-rigid shapes via high order statistics. *Axioms*, 3(3):300–319, 2014. 3
- [30] I. Talmi, R. Mechrez, and L. Zelnik-Manor. Template match-

- 1620 ing with deformable diversity similarity. In *Proc. of IEEE* 1674
1621 *Conf. on Computer Vision and Pattern Recognition*, pages 1675
1622 1311–1319, 2017. 2, 4, 7 1676
- 1623 [31] F. Tombari, S. Salti, and L. Di Stefano. Unique signatures of 1677
1624 histograms for local surface description. In *European conference 1678*
1625 on computer vision, pages 356–369. Springer, 2010. 1679
1626 3, 7 1680
- 1627 [32] A. Torsello. A game-theoretic approach to deformable shape 1681
1628 matching. In *Proceedings of the 2012 IEEE Conference on* 1682
1629 *Computer Vision and Pattern Recognition (CVPR)*, CVPR 1683
1630 ’12, pages 182–189, Washington, DC, USA, 2012. IEEE 1684
1631 Computer Society. 2, 3 1685
- 1632 [33] M. Vestner, Z. Lähner, A. Boyarski, O. Litany, R. Slossberg, 1686
1633 T. Remez, E. Rodola, A. Bronstein, M. Bronstein, R. Kimmel, et al. 1687
1634 Efficient deformable shape correspondence via 1688
1635 kernel matching. In *3D Vision (3DV), 2017 International* 1689
1636 *Conference on*, pages 517–526. IEEE, 2017. 2, 3 1690
- 1637 1691
- 1638 1692
- 1639 1693
- 1640 1694
- 1641 1695
- 1642 1696
- 1643 1697
- 1644 1698
- 1645 1699
- 1646 1700
- 1647 1701
- 1648 1702
- 1649 1703
- 1650 1704
- 1651 1705
- 1652 1706
- 1653 1707
- 1654 1708
- 1655 1709
- 1656 1710
- 1657 1711
- 1658 1712
- 1659 1713
- 1660 1714
- 1661 1715
- 1662 1716
- 1663 1717
- 1664 1718
- 1665 1719
- 1666 1720
- 1667 1721
- 1668 1722
- 1669 1723
- 1670 1724
- 1671 1725
- 1672 1726
- 1673 1727